frontiers in Physics

ORIGINAL RESEARCH
published: 04 April 2019
doi: 10.3389/fphy.2019.00047

Si/SiO_2 Core/Shell Luminescent Silicon Nanocrystals and Porous Silicon Powders With High Quantum Yield, Long Lifetime, and Good Stability

Bernard Gelloz[1]*, *Firman Bagja Juangsa*[2], *Tomohiro Nozaki*[2], *Koji Asaka*[1], *Nobuyoshi Koshida*[3] and *Lianhua Jin*[4]

[1] Graduate School of Engineering, Nagoya University, Nagoya, Japan, [2] School of Engineering, Tokyo Institute of Technology, Tokyo, Japan, [3] Graduate School of Engineering, Tokyo University of Agriculture and Technology, Tokyo, Japan, [4] Graduate School of Medicine and Engineering, University of Yamanashi, Kofu, Japan

Most of the highly efficient luminescent silicon nanocrystals (SiNCs) reported to date consist of organically capped silicon cores. Here, we report a method of obtaining Si/SiO_2 core/shell nanoparticles emitting at a peak energy of 1.5 eV with very high quantum yields (53–61%). The same method led to quantum yields of ∼30% for porous silicon powder emitting at 1.9 eV. The SiNCs were very stable under continuous excitation for several hours. The lifetime at 1.5 eV was over 232 μs, the longest ever reported for SiNCs, consistent with the very high luminescence efficiency. The SiNCs were first fabricated by non-thermal plasma synthesis or anodization in the case of porous silicon. Then, a thin oxide shell (∼1 nm) was grown using high-pressure water vapor annealing. This oxidation process allows for the growth of very good quality oxide with low defect concentration and low stress, resulting in very good surface passivation, which explains the very high quantum yields obtained.

Keywords: silicon nano crystals, porous silicon, luminescence, quantum yield, Core/shell

OPEN ACCESS

Edited by:
Petra Granitzer, University of Graz, Austria

Reviewed by:
Michael J. Sailor, University of California, San Diego, United States
Raul J. Martin-Palma, Autonomous University of Madrid, Spain

***Correspondence:**
Bernard Gelloz
gelloz@nuap.nagoya-u.ac.jp

Specialty section:
This article was submitted to Optics and Photonics, a section of the journal Frontiers in Physics

Received: *10 January 2019*
Accepted: *11 March 2019*
Published: *04 April 2019*

Citation:
Gelloz B, Juangsa FB, Nozaki T, Asaka K, Koshida N and Jin L (2019) Si/SiO_2 Core/Shell Luminescent Silicon Nanocrystals and Porous Silicon Powders With High Quantum Yield, Long Lifetime, and Good Stability. Front. Phys. 7:47. doi: 10.3389/fphy.2019.00047

INTRODUCTION

Luminescent Si nanocrystals (SiNCs) are intensively studied for their potential applications in diverse fields, such as optoelectronics, sensing, and medicine [1–20]. Some particularly important characteristics of such SiNCs include absolute quantum yield (AQY), stability, luminescence lifetime, surface chemistry, and synthesis route.

Anodization of Si wafers in hydrofluoric acid, leads to porous silicon (PSi) layers [21], which can then be milled to produce a powder of micrometer-sized flakes of nanostructures. Some degree of control of the micro-sized particles was achieved [22]. The photoluminescence (PL) of PSi is generally very broad, with full width at half maximum (FWHM) of 120–200 nm [12, 23], often explained by size distribution with quantum confinement as well as defect state emission [24]. The luminescence efficiency of PSi is generally rather low, and this was explained mainly by the existence of a small fraction of actually luminescent nano-crystallites [25]. AQY of 23% was reported with PSi layers treated by high-pressure water vapor annealing (HWA) [26, 27] and with PSi powders modified by solution-based chemical oxidation [28]. Recently, ∼32% was reported [14], for most

likely hydrogen-terminated PSi dried using a supercritical process. Hydrogen-terminated PSi is generally unstable due to the high reactivity of H-Si bonds. Growing good quality oxide helps with surface stabilization. In particular, HWA was proven very good at stabilizing PSi PL [26, 27], electroluminescence [29], photonic structures [30], and 2D Si photonic cavities [31]. Another very popular method is the substitution of hydrogen by organic groups. In particular, hydrosilylation was shown to be an effective way of stabilizing PSi optoelectronic materials and devices [32–34].

Another popular SiNCs fabrication route is plasma synthesis [15, 35, 36]. This route allows for better size control than PSi, and narrow emission lines were reported [37, 38]. The AQY generally decreases with the SiNC size [4, 9, 37]. AQYs much greater than those obtained with PSi were reported recently. Focusing on ensemble AQYs above ∼40%, SiNCs mostly consisted of Si cores whose surface was terminated by various kinds of organic compounds, alkyl groups attached by hydrosilylation being the most typical [2, 9, 10, 17, 19, 20]. The confinement somewhat depends on the type of organic group attached to the surface [20]. Due to the long organic chains, these organically-capped SiNCs usually take a paste (slurry-like) form, not ideal for electro- and opto-devices [39]. Moreover, they can easily agglomerate by phase separation when incorporated in a different matrix. Thus, for some applications, Si/SiO_2 core/shell SiNCs are preferred. For these nanoparticles, the highest reported AQY is ∼23%, obtained using PSi [26, 28].

The lifetime of the red emission of SiNCs typically ranges from microseconds to hundreds of microseconds, increasing with the emission wavelength [12, 23, 40, 41]. Such long lifetimes may be limiting in some applications, like those requiring high switching speeds, but they are actually an advantage for other applications such as gated imaging [5, 8].

As previously mentioned, HWA was used with PSi layers, leading to a quantum efficiency of 23% [26, 27] and very good PL and EL stability. These good performances were attributed to the very good quality and stable oxide layer (low defect concentration; low stress) passivating the PSi surface. In this paper, the effect of HWA on the optical properties of (i) SiNC powders prepared using non-thermal plasma synthesis, and (ii) PSi powders prepared by anodization followed by milling, were investigated. TEM, PL, AQYs, stability, and PL dynamics were investigated. The best results were obtained with the SiNCs, with very high AQYs, matching the highest values reported to date for organically terminated SiNCs, and very good stability. Furthermore, the lifetimes at given emission wavelengths were the longest ever observed.

EXPERIMENTAL

SiNC synthesis method and apparatus, as well as detailed reaction mechanisms, are provided elsewhere [36]. Briefly, a capacitively-coupled nonthermal plasma was generated by 70 MHz power source in a quartz tube reactor. $SiCl_4$ and H_2 mixture was used for precursor gas, while Ar was used as a balance so that the total pressure is maintained at 400 Pa. Excited H_2 abstracts chlorine from the chlorinated species ($SiCl_n$) which initiates nucleation of particles followed by their growth in the gas phase. The mean particle size is controllable by the reaction time. As-produced SiNCs have a chlorine-terminated surface which readily induces silicon suboxide surface upon exposing to air [35]. As-produced SiNCs were dry-etched by HF vapor to get fully hydrogen-terminated surfaces [42]. The final SiNCs exhibited a mean size of about 6 nm.

PSi layers of porosity 68% were formed by anodization in HF (55 wt. %):ethanol = 1:1 of silicon (100)-oriented wafers (5–10 Ω.cm) at 50 mA/cm^2. Anodization was performed for 21 min to produce 50 μm-thick layers. Immediately after formation, the PSi layers were separated from the substrate by applying a short high-current pulse. The PSi membranes thus obtained were dried and coarsely manually milled to produce the final powder.

In order to get a luminescent reference as-formed PSi layer for stability experiments, a 0.5 μm-thick PSi layer of porosity 80% was fabricated in HF (55 wt. %):ethanol = 1:2.67 at 10 mA/cm^2 for 100 s.

HWA was carried out using a 30.5 ml stainless steel main chamber. First, an about 1 mm thick carpet of dry SiNC powder (∼50 mg) was placed in a separate holder, which was then put into the main chamber. Water (0.54 ml) was then added in another part of the main chamber, not in contact with the SiNC powder. The main chamber was closed, heated to 260°C in order to set a water vapor pressure of 3.9 MPa in the chamber, and after 4 h it was allowed to cool down, and finally opened. The water was found to have condensed almost entirely at the surface of the lid (upper part) of the main chamber. Thus, the SiNC powder was only exposed to water vapor and was left in a dry state. It was extracted mechanically from the holder. The water did not show any color change to the naked eye and was disposed of. Notice that the system is scalable, and therefore it is possible to process larger amounts if needed. HWA-treated PSi and SiNCs will be referred to as HWA-PSi and HWA-SiNCs, respectively.

PL spectra were measured using a spectrometer (QEPro from Ocean Optics) with a spectral range of 200–1,000 nm and resolution of about 1 nm. Excitation was a light-emitting diode (LED) emitting at 385 nm (LLS-385 from Ocean Optics). Time-resolved PL measurements were acquired using a Horiba spectrofluorometer Fluoromax-4. PL stability was evaluated in the following way: powders were illuminated continuously for several hours by a laser diode emitting at 405 nm (85229-E0405-3CM; Edmund Optics; 1 mW on sample; spot diameter: 3 mm), while the PL intensity and laser power were measured every 10 min. The final result was the PL intensity divided by laser power. It turned out that the laser diode was quite stable.

AQY of powders were measured using the QEPro spectrometer and the LLS-385 LED, with an integrating sphere (Labsphere). The method is conventional and was also used by others. For instance, Jurbergs et al. [2] used a LED-380 with a USB2000 spectrometer and Joo et al. [14] used a LLS-365 with a QEPro spectrometer. In our case, the spectrometer's spectral response was calibrated with calibration lamp (Ocean Optics HL-2000-CAL-INT) in the 350–1,100 nm spectral range. We selected LLS-385, rather than LLS-365 (which

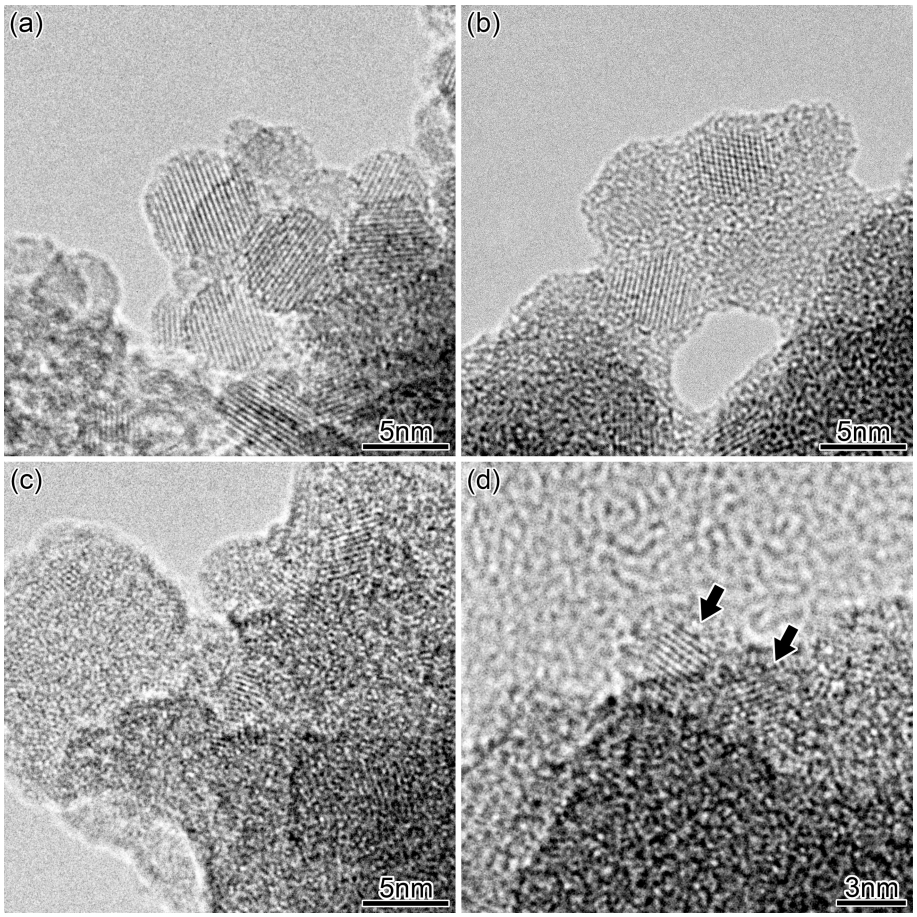

FIGURE 1 | TEM pictures of SiNCs before **(a)** and after HWA **(b)**. TEM pictures of PSi after HWA **(c,d)**. The arrows show the location of two nanocrystals.

we also own), as our excitation source because its emission spectrum fully overlaps the HL-2000-CAL-INT calibration range. As a base line, the intensity of the LED was measured with the integrating sphere containing an empty quartz cuvette (dimensions: 2 × 10 × 50 mm). Then the dried powder was introduced into the same cuvette, which was installed again in the integrating sphere in exactly the same position and orientation as for the base line measurement. Then a spectrum, consisting in the PL signal, and the LED signal was acquired. The absorption signal was derived from the decrease of the base line LED signal. Then the spectra were converted from power emission to photon number emission. The AQY, defined as the number of visible photons emitted per absorbed UV photon, was derived by taking the ratio between the integrated PL and absorption signals.

RESULTS AND DISCUSSION

The structures of the SiNCs and PSi powders were observed by transmission electron microscopy (TEM) using a JEOL JEM-2010 microscope, performed at an acceleration voltage of 120 kV. The TEM specimens were prepared by dropping the samples dispersed in isopropyl alcohol onto a microgrid. The lattice fringes with a spacing of 0.31 nm observed in nanoparticles correspond to the (111) planes of Si. The TEM image shown in **Figure 1a** reveals that the SiNCs are crystalline and mostly spherical. The average diameters of the SiNCs in **Figures 1a,b** are 5.5 and 4.7 nm, respectively. The as-formed sizes observed here are in agreement with earlier more detailed studies of similar powders, which established a mean size of 6 nm [36]. **Figures 1c,d** shows PSi after HWA. In **Figure 1c**, crystalline structures can be observed throughout the picture, suggesting the crystalline nature of the PSi structure was maintained by HWA. The diameter of the PSi particles indicated by the arrows in **Figure 1d** is approximately 2.7 nm, showing the sizes are much smaller in PSi than in our SiNCs. After HWA, the TEM image in **Figure 1b** shows the growth of an about 1 nm-thick amorphous oxide layer at the SiNCs surface, in agreement with a TEM study of HWA-treated silicon nanowires [43].

The PL spectra of the SiNC ensembles are shown in **Figure 2**. A large blue-shift was induced by HWA, as expected from the core size reduction by oxidation and quantum confinement effect. **Table 1** shows the PL characteristics of these spectra. Using the obtained peak energy, an attempt was made at roughly

estimating the SiNC mean size in each case using selected literature data [20, 44]. For HWA-SiNCs, the mean sizes are in rather good agreement with the values expected from TEM data and the previous size study of the as-formed SiNCs (see data in **Table 1**). The as-prepared SiNCs PL is rather broad, reflecting a consequent size distribution. After HWA, the PL became even broader, which can be attributed to an enlarged core size distribution, likely resulting from none-uniform oxide growth at the Si surface.

The PL of as-prepared PSi was extremely weak and, therefore, we do not show its characteristics in **Table 1**. The PL peak wavelength of HWA-PSi, about 650 nm, is typical of bright PSi layers. The PL peak is at a higher energy compared to that of the PL of HWA-SiNCs, suggesting that the mean size is much smaller in our PSi samples than in our SiNC powders. TEM data in **Figure 1** confirm this statement. The peak intensity was similar to that of HWA-SiNCs, but The FWHM was much smaller. The value, 137 nm, falls within the lower end of the typical values found for PSi layers [12, 14, 23, 40].

A picture of the HWA-PSi (left) and HWA-SiNC (right) powders in their cuvettes, placed under a handy UV lamp (SLUV-8 from As One; wavelength: 365 nm) is shown in **Figure 2**, when the excitation is on or off.

AQYs of HWA-PSi and HWA-SiNC powders were measured several times in order to get some statistical significance of measurements. Each time, the powder was unloaded from the cuvette and then reloaded, in order to average the parts of the powder exposed to the excitation. Measurements were also done on different days, re-calibrating the experiment each time. The PL intensity was linear with the excitation power, up to the maximum power incident on samples: 2 mW for a spot diameter of 7 mm (5.2 mW/cm^2). Therefore, there was no dependence of the AQY on the excitation power, in our experimental conditions. **Table 2** shows the results. Because the signal-to-noise ratio of the measured spectra was very good, the spread of measurement values given in **Table 2** gives the most significant uncertainty. The AQY of HWA-PSi and HWA-SiNC powders, were found in ranges 28–30.7% and 53–61.6%, respectively.

The lower AQY of HWA-PSi compared to HWA-SiNCs may be attributed to more significant exciton migration to regions having non-radiative defects because PSi is an interconnected network of nanocrystallites [12, 23, 40, 45]. However, considering the rather high extent of oxidation induced by HWA, the interconnection may not be that effective. A few reports have shown that the AQY decreases with SiNC size [4, 9, 37]. Then, the lower AQY of HWA-PSi may be because of its shorter peak emission wavelength. The ratio of the AQY of HWA-SiNCs by that of HWA-PSi is ∼56/29 ∼1.9. From the report of Mastronardi et al. [4], at 650 nm, the AQY was roughly 25% and for the maximum wavelength reported, 750 nm, it was 43%. This gives a ratio of 43/25 ∼1.7, which is similar to our ratio of 1.9, suggesting the lower efficiency of HWA-PSi compared to HWA-SiNCs could be due to this size effect.

For HWA-PSi, our values are close to the ∼32% recently reported by Joo et al. [14] who used supercritical drying to improve the AQY compared to when using air drying. Their PL peak wavelength was 685 nm, a bit higher than ours (650 nm), which may also explain their slightly higher AQY considering the emission wavelength dependence of the efficiency discussed above. Our results show that similarly high AQY (30% range) may be obtained without the sophisticated supercritical drying technique. Moreover, the HWA-grown oxide is rather relaxed and stable [26, 27], resulting in reasonably good PL stability as well.

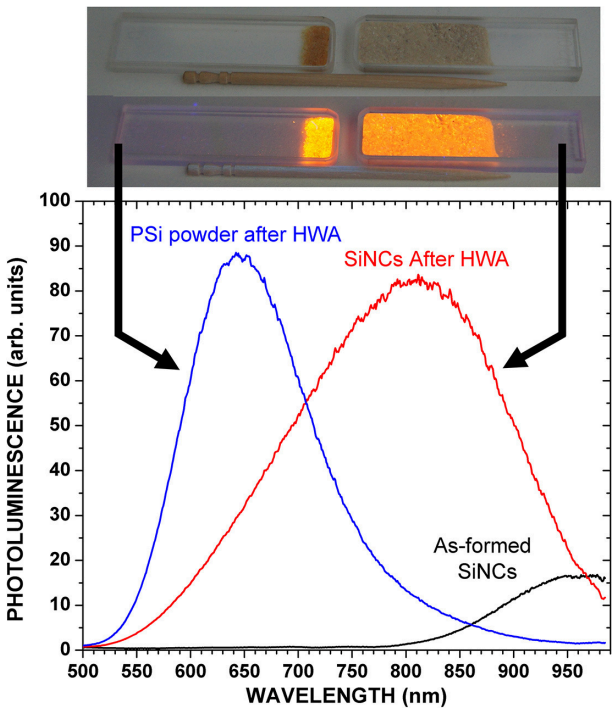

FIGURE 2 | PL of SiNCs powder before and after HWA, and of PSi powder after HWA. Excitation was 385 nm. Pictures of the powders under a 365 nm lamp (SLUV-8 from As One) are shown when the lamp was off and on.

Considering AQYs of HWA-SiNCs, our values match the highest reported ones, in the 50–60% range [2, 7, 9, 10, 17, 19]. Most highly efficient SiNCs were obtained using organic surface passivation [2, 9, 10, 17, 19]. However, our HWA-SiNCs distinguish themselves from these studies in the fact that they are oxide-passivated.

Figure 3 shows the PL intensity as a function of time under continuous excitation in air. The as-formed luminescent PSi layer shows that hydrogen-terminated SiNCs are not stable, and shows a spectacular drop in the initial stage of the experiment. Typically, such silicon surfaces easily get oxidized in air. In contrast, HWA-treated samples are much more stable in air. The oxide is not only providing good passivation but is also stable right after HWA, with no strong evolution of its structure. This is in agreement with previous results of PSi PL [26, 27] and EL [29] of PSi layers treated by HWA.

Figure 4 shows the PL decays across the PL spectrum for HWA-SiNCs excited at 365 nm. They are multi-exponential, which is typical for SiNCs. The departure from a single exponential behavior is typically explained by the

TABLE 1 | PL peak wavelength and energy and FWHM of indicated powders, from spectra shown in **Figure 2**, and estimated mean size according to measurements and literature.

Powder	FWHM (nm)	Peak λ Peak *E*	Mean diameter (nm): from present and previous [36] TEM	Mean diameter (nm): from literature
SiNCs	170*	960 nm 1.29 eV	~6	~ 6.3 (Ref. 1)
HWA-SiNCs	240	825 nm 1.50 eV	~4	~4 (Ref. 1)
HWA-Psi	137	650 nm 1.91 eV	~2.7	~2.75 (Ref. 2)

*The data of Ref. 1 [20] do not cover the emission energy of 1.91 eV, so the datum for this energy was taken from Ref 2 [44]. *Obtained by doubling the half width at half maximum.*

TABLE 2 | AQYs of fabricated powders.

Powder	*N*	Mean (%)	Std dev. (%)	Min (%)	Median (%)	Max (%)
HWA-PSi	5	29.1	1.3	28.0	28.5	30.7
HWA-SiNCs	12	55.75	2.49	53.00	55.45	61.60

N is the number of independent measurements done with different powder samples.

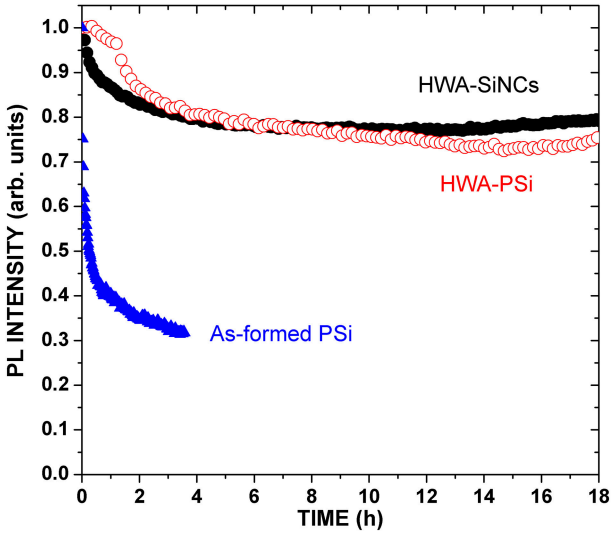

FIGURE 3 | PL peak intensity of HWA-treated SiNCs and PSi powders, as well as of an as-formed 80%-porosity PSi layer, as a function of time under continuous excitation at 405 nm (1 mW on sample; spot diameter: 3 mm).

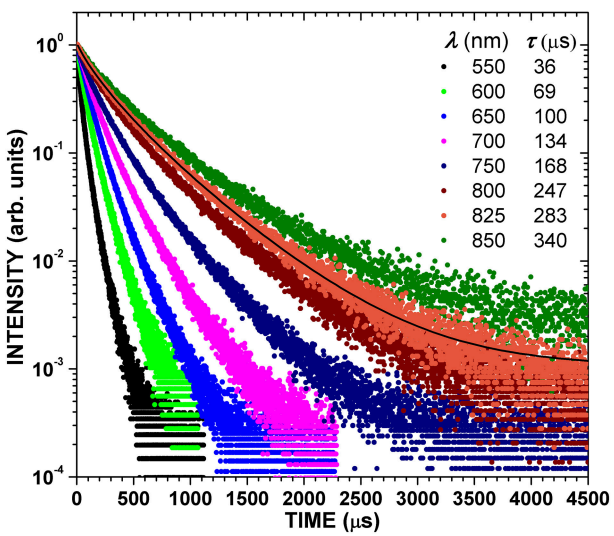

FIGURE 4 | Time-resolved PL of HWA-treated SiNCs at indicated wavelengths. Indicated lifetimes correspond to the time taken for the PL to fall by a factor of *e*. The black solid curve is a fit with a stretched exponential.

inhomogeneous nature of the PL spectrum, invoking crystallite shape distributions or exciton migration [12, 23, 40], or energy transfer between nanocrystals [46]. Exciton migration is not likely to have a large effect for our HWA-SiNC powders since the surface oxide should prevent it. The decays could be fitted with a stretched exponential $\exp[-(t/\tau)^{\beta}]$ [40, 45]. However, parameter β was found to vary significantly, from ~0.76 at 825 nm to ~0.4 at 550 nm, altering the practical meaning of τ. Thus, a more practical estimation of the decay time was used: the time taken for the PL to fall by a factor of *e*. [40, 47] Obtained values are shown in **Figure 4**. At the PL peak wavelength, 825 nm, this method gives 283 μs, whereas the stretched exponential gives $\tau = 232$ μs with $\beta = 0.75$ (fit shown in **Figure 4**). The two values are not too far apart as β is not too low in this case. τ increases with the wavelength, which is a typical behavior in SiNC ensembles, and was attributed to size-dependent quantum confinement effects [40], though size-dependent surface defects may also play a role [4].

The PL lifetime in SiNCs, τ, has been estimated as $(\tau_r^{-1} + \tau_{nr}{}^{-1})^{-1}$, where τ_r and τ_{nr} are the radiative and non-radiative lifetimes, respectively, [12, 23, 40]. Thus, τ is expected to increase with the AQY since τ_{nr} decreases. Thus, we can compare our lifetimes, in particular that at 825 nm, with those reported for SiNCs exhibiting high AQYs. For example, Sanghaleh et al. [10] reported τ ~90 μs at 860 nm, for an AQY of 60 ± 5%. Mastronardi et al. [4] reported τ ~60 μs at 700 nm, for an AQY of 43%. A lifetime of ~125 μs at ~825 nm was reported for alkyl-terminated SiNCs with AQY of ~65% [19]. A lifetime of ~155 μs at ~860 nm was reported also for alkyl-terminated SiNCs with maximum AQY of ~39% [48]. Furthermore, τ ~65 μs at 800 nm, for PSi having an AQY of 32% (peak wavelength 685 nm) [14]. A particular study of PL lifetimes in SiNCs [41] reported τ ~131 μs at 815 nm for dodecyl-capped SiNCs. The better the surface passivation is, the lower τ_{nr}, the higher τ, and the higher the AQY are. Thus, our very long PL decays are consistent with our very high measured AQYs, which can be attributed to very good surface passivation provided by the oxide generated by HWA.

The high AQY and good stability are consistent with those we had obtained previously using HWA with PSi layers [26, 27]. In these reports dedicated to PSi layers treated by HWA, we have shown that HWA produces a relaxed, and thus stable, oxide. In addition, electron spin resonance showed very low defect concentration at the core/shell interface [26].

CONCLUSION

AQYs in ranges 53–61 and 28–30% were measured for SiNCs and PSi powders treated by HWA, respectively. These values are in the higher range of currently reported AQYs [2, 7, 9, 10, 14, 17, 19]. However, our SiNCs are the only ones passivated with oxide to show such high AQYs to date, most others being terminated by some kind of organic groups [2, 9, 10, 17, 19]. At the PL peak emission wavelength (825 nm), the lifetime of HWA-SiNCs was 232 μs using a stretched exponential, or 283 μs using a decay by 1/*e*, the highest values ever reported at this wavelength. They were also very stable under continuous optical excitation. These oxide-passivated SiNCs may find some applications in gated imaging [5, 8], optoelectronic devices [3, 15, 49, 50], and systems using light emission of nano-particles.

DATA AVAILABILITY

All datasets generated for this study are included in the manuscript and/or the supplementary files.

AUTHOR CONTRIBUTIONS

BG intitiated the study with TN, did all the optical measurements, managed the discussion and wrote the article. FBJ setup the nanocrystals synthesis system and supplied the nanocrystals. TN heads the laboratory where the Si nanocrystals were fabricated. He participated in various discussions. KA did all the TEM experiments and related disussions. NK participated in various discussions about the oxidizing treatment (HWA). LJ participated in various discussions, supported experiments, and treatments of the silicon nanocrystals.

ACKNOWLEDGMENTS

This work was partially supported by grant-in-aid for Scientific Research C (16K04898) and B (18H01378) from JSPS, Japan. The authors thank Y. Saito for help with TEM, and H. Kishida for his assistance in time-resolved PL experiments, in Nagoya University. FBJ acknowledges the Indonesia Endowment Fund for Education (LPDP) for their support of this study.

REFERENCES

1. Gelloz B, Koshida N. Electroluminescence with high and stable quantum efficiency and low threshold voltage from anodically oxidized thin porous silicon diode. *J Appl Phys.* (2000) **88**:4319–24. doi: 10.1063/1.1290458
2. Jurbergs D, Rogojina E, Mangolini L, Kortshagen U. Silicon nanocrystals with ensemble quantum yields exceeding 60%. *Appl Phys Lett.* (2006) **88**: 233116. doi: 10.1063/1.2210788
3. Cheng KY, Anthony R, Kortshagen UR, Holmes RJ. High-efficiency silicon nanocrystal light-emitting devices. *Nano Lett.* (2011) **11**:1952–6. doi: 10.1021/nl2001692
4. Mastronardi ML, Maier-Flaig F, Faulkner D, Henderson EJ, Kubel C, Lemmer U, et al. Size-dependent absolute quantum yields for size-separated colloidally-stable silicon nanocrystals. *Nano Lett.* (2012) **12**:337–42. doi: 10.1021/nl2036194
5. Gu L, Hall DJ, Qin ZT, Anglin E, Joo J, Mooney DJ, et al. *In vivo* time-gated fluorescence imaging with biodegradable luminescent porous silicon nanoparticles. *Nat Commun.* (2013) **4**:2326. doi: 10.1038/ncomms3326
6. Canham LT. *Handbook on Porous Silicon Springer.* Heidelberg; New York, NY; Dordrecht; London: Springer International Publishing Switzerland) (2014). doi: 10.1007/978-3-319-05744-6
7. Cho B, Baek S, Woo HG, Sohn H. Synthesis of silicon quantum dots showing high quantum efficiency. *J Nanosci Nanotechnol.* (2014) **14**:5868–72. doi: 10.1166/jnn.2014.8297
8. Joo J, Liu XY, Kotamraju VR, Ruoslahti E, Nam Y, Sailor MJ. Gated luminescence imaging of silicon nanoparticles. *ACS Nano.* (2015) **9**:6233–41. doi: 10.1021/acsnano.5b01594
9. Rinck J, Schray D, Kubel C, Powell AK, Ozin GA. Size-dependent oxidation of monodisperse silicon nanocrystals with allylphenylsulfide surfaces. *Small.* (2015) **11**:335–40. doi: 10.1002/smll.201401965
10. Sangghaleh F, Sychugov I, Yang ZY, Veinot JGC, Linnros J. Near-unity internal quantum efficiency of luminescent silicon nanocrystals with ligand passivation. *ACS Nano.* (2015) **9**:7097–104. doi: 10.1021/acsnano.5b01717
11. Zhou S, Pi XD, Ni ZY, Ding Y, Jiang YY, Jin CH, et al. Comparative study on the localized surface plasmon resonance of boron- and phosphorus-doped silicon nanocrystals. *ACS Nano.* (2015) **9**:378–86. doi: 10.1021/nn505416r
12. Gelloz B. Luminescent Properties of Porous Silicon. In: Korotcenkov G, editor. *Porous Silicon: From Formation to Application: Formation and Properties*, Vol 1 (Boca Raton: CRC Press, TaylorandFrancis Group) (2016). p. 187–216.
13. Gelloz B. Electroluminescence devices (LED). In: Korotcenkov G, *Porous Silicon: From Formation to Application,* Vol 3, (Boca Raton: CRC Press, TaylorandFrancis Group) (2016). p. 3–34. doi: 10.1201/b19042-3
14. Joo J, Defforge T, Loni A, Kim D, Li ZY, Sailor MJ, et al. Enhanced quantum yield of photoluminescent porous silicon prepared by supercritical drying. *Appl Phys Lett.* (2016) **108**:153111. doi: 10.1063/1.4947084
15. Kortshagen UR, Sankaran RM, Pereira RN, Girshick SL, Wu JJ, Aydil ES. Nonthermal plasma synthesis of nanocrystals: fundamental principles, materials, and applications. *Chem Rev.* (2016) **116**:11061–127. doi: 10.1021/acs.chemrev.6b00039
16. Zhou S, Ni ZY, Ding Y, Sugaya M, Pi XD, Nozaki T. Ligand-free, colloidal, and plasmonic silicon nanocrystals heavily doped with boron. *Acs Photonics.* (2016) **3**:415–22. doi: 10.1021/acsphotonics.5b00568
17. Islam MA, Mobarok MH, Sinelnikov R, Purkait TK, Veinot JGC. Phosphorus pentachloride initiated functionalization of silicon nanocrystals. *Langmuir.* (2017) **33**:8766–73. doi: 10.1021/acs.langmuir.7b00518
18. Kim D, Kang J, Wang T, Ryu HG, Zuidema JM, Joo J, et al. Two-photon *in vivo* imaging with porous silicon nanoparticles. *Adv Mater.* (2017) 29:1703309. doi: 10.1002/adma.201703309
19. Marinins A, Shafagh RZ, van der Wijngaart W, Haraldsson T, Linnros J, Veinot JGC, et al. Light-converting polymer/si nanocrystal composites with stable 60–70% quantum efficiency and their glass laminates. *Acs Appl Mater Interfaces.* (2017) **9**:30267–72. doi: 10.1021/acsami.7b09265
20. Carroll GM, Limpens R, Neale NR. Tuning confinement in colloidal silicon nanocrystals with saturated surface ligands. *Nano Lett.* (2018) **18**:3118–24. doi: 10.1021/acs.nanolett.8b00680
21. Canham LT. Silicon quantum wire array fabrication by electrochemical and chemical dissolution of wafers. *Appl Phys Lett.* (1990) **57**:1046–8. doi: 10.1063/1.103561
22. Qin ZT, Joo J, Gu L, Sailor MJ. Size control of porous silicon nanoparticles by electrochemical perforation etching. *Part Part Syst Charact.* (2014) **31**:252–6. doi: 10.1002/ppsc.201300244
23. Gelloz B. Photoluminescence of Porous Silicon. In: Canham L. *Handbook on Porous Silicon*, Heidelberg; New York, NY; Dordrecht; London: Springer International Publishing Switzerland) (2014). p. 307–20.
24. Schmidt T, Chizhik AI, Chizhik AM, Potrick K, Meixner AJ, Huisken F. Radiative exciton recombination and defect luminescence

observed in single silicon nanocrystals. *Phys Rev B.* (2012) **86**:125302. doi: 10.1103/PhysRevB.86.119906
25. Credo GM, Mason MD, Buratto SK. External quantum efficiency of single porous silicon nanoparticles. *Appl Phys Lett.* (1999) **74**:1978–80. doi: 10.1063/1.123719
26. Gelloz B, Kojima A, Koshida N. Highly efficient and stable luminescence of nanocrystalline porous silicon treated by high-pressure water vapor annealing. *Appl Phys Lett.* (2005) **87**:031107. doi: 10.1063/1.2001136
27. Gelloz B, Koshida N. Mechanism of a remarkable enhancement in the light emission from nanocrystalline porous silicon annealed in high-pressure water vapor. *J Appl Phys.* (2005) **98**:123509. doi: 10.1063/1.2147847
28. Joo J, Cruz JF, Vijayakumar S, Grondek J, Sailor MJ. Photoluminescent porous Si/SiO2 core/shell nanoparticles prepared by borate oxidation. *Adv Funct Mater.* (2014) **24**:5688–94. doi: 10.1002/adfm.201400587
29. Gelloz B, Shibata T, Koshida N. Stable electroluminescence of nanocrystalline silicon device activated by high pressure water vapor annealing. *Appl Phys Lett.* (2006) **89**:191103. doi: 10.1063/1.2385206
30. Gelloz B, Koshida N. Stabilization and operation of porous silicon photonic structures from near-ultraviolet to near-infrared using high-pressure water vapor annealing. *Thin Solid Films.* (2010) **518**:3276–9. doi: 10.1016/j.tsf.2009.08.043
31. Fujita M, Gelloz B, Koshida N, Noda S. Reduction in surface recombination and enhancement of light emission in silicon photonic crystals treated by high-pressure water-vapor annealing. *Appl. Phys. Lett.* (2010) **97**:121111. doi: 10.1063/1.3489419
32. Buriak JM. Organometallic chemistry on silicon and germanium surfaces. *Chem Rev.* (2002) **102**:1271–308. doi: 10.1021/cr000064s
33. Gelloz B, Sano H, Boukherroub R, Wayner DDM, Lockwood DJ, Koshida N. Stabilization of porous silicon electroluminescence by surface passivation with controlled covalent bonds. *Appl Phys Lett.* (2003) **83**:2342–4. doi: 10.1063/1.1613812
34. Ghulinyan M, Gelloz B, Ohta T, Pavesi L, Lockwood DJ, Koshida N. Stabilized porous silicon optical superlattices with controlled surface passivation. *Appl Phys Lett.* (2008) **93**:061113. doi: 10.1063/1.2969294
35. Gresback R, Nozaki T, Okazaki K. Synthesis and oxidation of luminescent silicon nanocrystals from silicon tetrachloride by very high frequency nonthermal plasma. *Nanotechnology.* (2011) **22:**305605. doi: 10.1088/0957-4484/22/30/305605
36. Ding Y, Yamada R, Gresback R, Zhou S, Pi XD, Nozaki T. A parametric study of non-thermal plasma synthesis of silicon nanoparticles from a chlorinated precursor. *J Phys D-Appl Phys.* (2014) **47**:28**.** doi: 10.1088/0022-3727/47/48/485202
37. Miller JB, Van Sickle AR, Anthony RJ, Kroll DM, Kortshagen UR, Hobbie EK. Ensemble brightening and enhanced quantum yield in size-purified silicon nanocrystals. *ACS Nano.* (2012) **6**:7389–96. doi: 10.1021/nn302524k
38. Sychugov I, Fucikova A, Pevere F, Yang ZY, Veinot JGC, Linnros J. Ultranarrow luminescence linewidth of silicon nanocrystals and influence of matrix. *Acs Photonics.* (2014) **1**:998–1005. doi: 10.1021/ph500221z
39. Angi A, Loch M, Sinelnikov R, Veinot JGC, Becherer M, Lugli P, et al. The influence of surface functionalization methods on the performance of silicon nanocrystal LEDs. *Nanoscale.* (2018) **10**:10337–42. doi: 10.1039/C7NR09525B
40. Cullis AG, Canham LT, Calcott PDJ. The structural and luminescence properties of porous silicon. *J Appl Phys.* (1997) **82**:909–65. doi: 10.1063/1.366536
41. Yang Z, De los Reyes GB, Titova LV, Sychugov I, Dasog M, Linnros J, et al. Evolution of the ultrafast photoluminescence of colloidal silicon nanocrystals with changing surface chemistry. *Acs Photonics.* (2015) **2**:595–605. doi: 10.1021/acsphotonics.5b00143
42. Ding Y, Gresback R, Liu Q, Zhou S, Nozaki T. Development of efficient silicon nanocrystal and conjugated polymer hybrid solar cells. *Nano Energy.* (2014) **9**:25–31. doi: 10.1016/j.nanoen.2014.06.024
43. Salhi B, Gelloz B, Koshida N, Patriarche G, Boukherroub R. Synthesis and photoluminescence properties of silicon nanowires treated by high-pressure water vapor annealing. *Phys Stat Solidi a-Appl Mater Sci.* (2007) **204**:1302–6. doi: 10.1002/pssa.200674321
44. Wolkin MV, Jorne J, Fauchet PM, Allan G, Delerue C. Electronic states and luminescence in porous silicon quantum dots: the role of oxygen. *Phys Rev Lett.* (1999) **82**:197–200. doi: 10.1103/PhysRevLett.82.197
45. Bisi O, Ossicini S, Pavesi L. Porous silicon: a quantum sponge structure for silicon based optoelectronics. *Surf Sci Rep.* (2000) **38**:5–126. doi: 10.1016/S0167-5729(99)00012-6
46. Jayatilleka H, Diamare D, Wojdak M, Kenyon AJ, Mokry CR, Simpson PJ, et al. Probing energy transfer in an ensemble of silicon nanocrystals. *J. Appl. Phys.* (2011) **110**:033522. doi: 10.1063/1.3622151
47. Xie YH, Wilson WL, Ross FM, Mucha JA, Fitzgerald EA, Macaulay JM, et al. Luminescence and structural study of porous silicon films. *J Appl Phys.* (1992) **71**:2403–7. doi: 10.1063/1.351097
48. Beri D, Busko D, Mazilkin A, Howard IA, Richards BS, Turshatov A. Highly photoluminescent and stable silicon nanocrystals functionalized via microwave-assisted hydrosilylation. *RSC Adv.* (2018) **8**:9979–84. doi: 10.1039/C7RA13577G
49. Ding Y, Sugaya M, Liu QM, Zhou S, Nozaki T. Oxygen passivation of silicon nanocrystals: influences on trap states, electron mobility, and hybrid solar cell performance. *Nano Energy.* (2014) **10**:322–8. doi: 10.1016/j.nanoen.2014.09.031
50. Ding Y, Nozaki T. Silicon Nanocrystal-based organic/inorganic hybrid solar cells. In: Ikhmayies S, editor. *Advances in Silicon Solar Cells*. Cham: Springer. (2018). p.177–203.

Conflict of Interest Statement: The authors declare that the research was conducted in the absence of any commercial or financial relationships that could be construed as a potential conflict of interest.